

**JOUL, Volume 3**

**Supplemental Information**

**Electrosynthesis of Hydrogen Peroxide**

**by Phase-Transfer Catalysis**

**Alexander T. Murray, Sahag Voskian, Marcel Schreier, T. Alan Hatton, and Yogesh Surendranath**

## Table of Contents

Title	Pages
<b>Materials and Chemicals</b>	<b>S2</b>
<b>General Batch Electrochemical Methods</b>	<b>S2</b>
<b>UV-Vis Spectroscopy of Phase Transfer and Peroxide Production</b>	<b>S3</b>
<b>NMR Spectroscopy Quantitation of Hexanol/Water Immiscibility</b>	<b>S3</b>
<b>Flow Reactor Design and Operation</b>	<b>S4-10</b>
<b>Reverse Osmosis Energy Calculations</b>	<b>S10</b>
<b>Table S1.</b> Priming solutions in surge tanks	<b>S6</b>
<b>Table S2.</b> Flow rates for each experiment	<b>S8</b>
<b>Figure S1:</b> Representative aqueous UV-Vis spectra of AQDSNa <sub>2</sub> and AQDSH <sub>2</sub> Na <sub>2</sub>	<b>S11</b>
<b>Figure S2.</b> <sup>1</sup> H NMR spectrum of D <sub>2</sub> O after mixing with 0.1 M TBACl/1-hexanol	<b>S11</b>
<b>Figure S3.</b> Phase transfer coefficient for AQDSNa <sub>2</sub> /AQDSH <sub>2</sub> Na <sub>2</sub> into CH <sub>2</sub> Cl <sub>2</sub>	<b>S12</b>
<b>Figure S4.</b> UV-Vis spectrum of electrolyte-free water upon mixing with AQDSH <sub>2</sub> TBA <sub>2</sub> /1-hexanol	<b>S12</b>
<b>Figure S5.</b> UV/visible spectrum of quinone before and after a cycle of reduction, phase transfer, reoxidation and back transfer	<b>S13</b>
<b>Figure S6.</b> Detailed process flow diagram	<b>S13</b>
<b>Figure S7.</b> Diagram of the first mixer-settler <b>MS-1</b>	<b>S14</b>
<b>Figure S8.</b> Picture of the second mixer-settler <b>MS-2</b>	<b>S14</b>
<b>Figure S9.</b> Schematic and illustrations of electrochemical cell	<b>S15</b>
<b>Figure S10.</b> Current-potential relationship of the cell operated in a flow configuration	<b>S16</b>
<b>Figure S11.</b> Increase in H <sub>2</sub> O <sub>2</sub> concentration with time and current density vs. time for the flow cell operated in a looped configuration	<b>S16</b>
<b>Figure S12.</b> Power densities of electrochemical cell and Faradaic efficiencies for H <sub>2</sub> O <sub>2</sub> production without iR correction.	<b>S17</b>
<b>References</b>	<b>S18</b>

## Materials and Chemicals

2,7-disodium anthraquinone disulfonate monohydrate (ACS Grade) was obtained from TCI Chemicals and used as received. Perchloric acid (99.9995%), sodium hydroxide (99.995%, semiconductor grade), tetrabutylammonium chloride (99%), tetrabutylammonium bromide (99%), and disodium EDTA (99%) were obtained from Sigma-Aldrich and used as received. Citric acid (99%) was obtained from VWR and used as received. Aqueous solutions were produced using Milli-Q 18.2 M $\Omega$  cm<sup>-2</sup> water. 1-hexanol (ACS grade) was obtained from Sigma-Aldrich and used as received. Carbon felt, G100 Soft Graphite Battery Felt, was obtained from AvCarb, and nickel foam was obtained from Xiamen Tmax battery supplies (6 mm thickness). Graphite rods (150 x 6 mm, 99.999%) were obtained from Sigma-Aldrich, Pt mesh (99.995%) and wire (99.995%) were obtained from Alfa-Aesar, and Ag/AgCl leakless reference electrodes were obtained from eDAQ. Bipolar membranes were manufactured by Fumasep, purchased from the Fuel Cell Store, and soaked in aqueous 1.0 M NaCl when not in use.

## General Batch Electrochemical Methods

All electrochemical experiments were conducted at ambient temperature ( $21 \pm 1$  °C) using a Biologic VSP 16-channel potentiostat and a three-electrode electrochemical cell with a porous glass frit separating the working and auxiliary compartments. Unless otherwise stated, a platinum mesh was used as the counter electrode. Leakless Ag/AgCl reference electrodes were used for experiments conducted in acidic electrolytes, and stored in Millipore® water when not in use. Reference electrodes were periodically checked relative to pristine reference electrodes to ensure against potential drift. Electrode potentials were converted to the RHE scale using  $E(\text{RHE}) = E(\text{Ag}/\text{AgCl}) + 0.197 \text{ V} + 0.059 \times \text{pH} \text{ V}$ . Cyclic voltammograms were recorded using a glassy carbon working electrode in quiescent N<sub>2</sub>-sparged electrolyte and produced the data in Figure 3a. Bulk electrolyses were performed at a constant applied potential of  $-0.1$  to  $-0.2$  V vs RHE using a 150 x 6 mm graphite rod working electrode. The electrolyte in the working compartment was stirred at 600 rpm and the bulk electrolysis was terminated when the current dropped below 0.7 mA and the dark characteristic color of the semiquinone (formed by comproportionation) disappeared. Uncompensated resistances,  $R_u$ , were generally under 30  $\Omega$  and were ignored.

## UV-Vis Spectroscopy of Phase Transfer and Peroxide Production

UV-Vis spectra were collected on a Varian Cary 50 UV/Visible spectrometer, with manual baseline correction. Starna quartz cells with a 1 cm path length were used for all measurements and were capped with septa. To quantify the extent of phase transfer of the oxidized anthraquinone 2,7-disulfonate (AQDS<sup>2-</sup>), 20 mM AQDSNa<sub>2</sub> in 0.1 M HClO<sub>4</sub> was shaken with the appropriate concentration of TBACl in 1-hexanol (50 mM to 300 mM, Figure 3b) and allowed to separate for 5 minutes. Subsequently, the amount of quinone remaining in the aqueous layer was measured by UV-Vis spectroscopy using the known extinction coefficient,  $\epsilon$ , of  $5.7 \times 10^3 \text{ M}^{-1} \text{ cm}^{-1}$  at 328 nm.<sup>1</sup> To quantify the extent of phase transfer of the reduced dihydroanthraquinone 2,7-disulfonate (AQDSH<sub>2</sub><sup>2-</sup>), the following procedure was followed. First, 20 mM AQDSH<sub>2</sub>Na<sub>2</sub> in 0.1 M HClO<sub>4</sub> was prepared by bulk electrolysis (see details above) of 20 mM AQDSNa<sub>2</sub> in 0.1 M HClO<sub>4</sub> in a N<sub>2</sub>-filled 'wet' glove box. The resulting aqueous AQDSH<sub>2</sub>Na<sub>2</sub> solution was shaken with the appropriate concentration of TBACl in 1-hexanol (50 mM to 300 mM, Figure 3b) and allowed to separate for 5 minutes. The resulting aqueous phase was removed from the glove box and bubbled with O<sub>2</sub> for 2 minutes, then stirred under air for 20 minutes to quantitatively oxidize AQDSH<sub>2</sub>Na<sub>2</sub> to AQDSNa<sub>2</sub>. The absorbance at 328 nm was measured to infer the concentration of AQDSH<sub>2</sub>Na<sub>2</sub> remaining in the aqueous phase following phase transfer. This procedure generated the partition fraction data reported in Figure 3b.

The reaction of AQDSH<sub>2</sub><sup>2-</sup> with O<sub>2</sub> as followed by UV-Vis spectroscopy (Figure 3c). For this experiment, 20 mM AQDSNa<sub>2</sub> in 0.1 M HClO<sub>4</sub> was fully reduced via bulk electrolysis at 2.25 V applied potential in the 26 cm<sup>2</sup> bipolar flow cell described below (p. S5), under N<sub>2</sub> at 10 mL min<sup>-1</sup> flow rate, until the current dropped below 5 mA. The reduced quinone AQDSH<sub>2</sub>Na<sub>2</sub> was then extracted into 0.1 M TBACl in 1-hexanol under N<sub>2</sub>. The organic 1-hexanol phase was transferred into a cuvette that was purged with N<sub>2</sub> and the first spectrum of the fully reduced quinone was recorded. The cap of the cuvette was then removed to expose the sample to atmospheric O<sub>2</sub> and permit slow oxidation of the reduced quinone. Spectra were recorded every 2 minutes (Figure 3c). The full oxidation was achieved within 25 minutes.

## NMR Spectroscopy Quantitation of Hexanol/Water Immiscibility

In order to determine the amount TBACl/1-hexanol that is carried into the pure aqueous phase, <sup>1</sup>H NMR spectra were collected on a Bruker Avance 401 spectrometer, at 400 MHz (<sup>1</sup>H) and referenced to the residual undeuterated solvent peak. Relaxation delay was set to 20 s to avoid selective saturation effects. An equal volume of D<sub>2</sub>O was mixed with 0.1 M TBACl/1-hexanol and this was stirred for 10 minutes then centrifuged for 10 minutes at 7000 rpm. An internal standard of methanol (0.5%) was added. The D<sub>2</sub>O layer was then analysed by <sup>1</sup>H NMR spectroscopy (Figure S2) which revealed <1 mg mL<sup>-1</sup> transfer of 1-hexanol to the aqueous phase.

## Flow Reactor Design and Operation

The flow system for the continuous electrochemical production of hydrogen peroxide consists of two mixer-settlers (MS), an electrochemical cell and four main streams. As seen in Figure S6, the aqueous catholyte stream (blue) carries the reduced anthraquinone from the electrochemical cell to the organic stream and the oxidized anthraquinone from the organic stream back to the electrochemical cell. The organic stream (red) carries the reduced anthraquinone to the oxygen-water reaction zone and the oxidized anthraquinone back from the reaction zone. The water stream (green) enters the reaction zone where it is sparged with O<sub>2</sub> and contacted with reduced anthraquinone, then carries hydrogen peroxide out of the reaction zone. The aqueous anolyte stream (orange) circulates through the anodic half-cell. The streams are pumped using eight pump heads connected to four pump drives. Five surge tanks are used to buffer fluctuations in the flow rate and gas inlet pressure. After the mixing and settling in MS-2, the organic phase carries the oxidized quinone back into MS-1, where it partitions among the two phases. This introduces freshly oxidized quinone into the catholyte which is reduced again in the electrochemical cell.

### *Electrochemical cell:*

A custom flow electrochemical cell was fabricated as shown in Figure S9. Two 3" × 3", 1/8" thick, 316 stainless steel sheets were used as current collectors. Two 3" × 3", 1/2" thick, high-temperature silicone rubber sheets (50A Durometer) were used to make the anodic and cathodic half cells. Cavities (2" × 2", 25.8 cm<sup>2</sup>) were made in the silicone sheets to accommodate the electrode material; four stacked 2" × 2" graphite battery felt pieces served as the cathode, and three stacked 2" × 2" nickel foam sheets as the anode. Polypropylene inlet and outlet fittings were inserted into the sides of the silicone sheets to allow for anolyte and catholyte circulation flows. The two half-cells were separated by a 3" × 3" bipolar membrane of which 2" × 2" was exposed, giving an active area of 4 sq inch (25.8 cm<sup>2</sup>).

Electrochemical analysis was performed potentiostatically using a VersaSTAT 3 Potentiostat Galvanostat from Ametek®, and the results were analysed in VersaStudio (Princeton Applied Research).

### *Pumps and tubing:*

The flow system shown in Figure S6 was controlled by four Masterflex L/S II digital drive peristaltic pumps purchased from Cole-Palmer, each with a double head, allowing for eight streams to be pumped through 14 gauge Masterflex Viton® tubes. Tubing used in the system was 1/8" ID Versilion® and Tygon® tubing for organic and aqueous streams respectively.

### *Surge tanks:*

The surge tanks were used to buffer the small fluctuations and drifts in flow rates of the streams which would otherwise disturb the level control in the settling zones of the mixer-settlers. This was done by constantly adjusting the flow rates to maintain the liquid levels in the tanks and maintain equal volumes of each phase in the mixer-settlers. This is mainly due to the small flow rates considered in this work (2.5–20 mL min<sup>-1</sup>). At higher flow rates, the relative error in flow would be insignificant and the need for surge tanks would be obviated.

### *Mixer-settlers:*

The process involves two mixer-settlers. The first (MS-1), allows the mixing of the catholyte with the organic phase, the second (MS-2) allows the mixing of the water stream with the organic phase while being sparged with O<sub>2</sub> (Figure 5).

MS-1 was machined from polypropylene (Figure S7). The mixing zone was a cylindrical cup, with liquid inlets on both sides at the bottom, and was separated from the settling zone by an emulsion overflow and a baffle. The settling zone had three coalescence plates, to enhance phase separation, and a light phase weir to allow for level fluctuations. The volumes of the mixing and settling zones were ~ 100 mL each, resulting in a total holdup volume of ~ 200 mL.

MS-2 was custom made by James Glass Inc. (Figure S8). The mixing chamber was covered with a cap that had ports to allow for gas flow in and out of the mixing chamber. The O<sub>2</sub> flow was introduced to the center of the mixing zone through a gas dispersion tube with a porous fritted glass tip. The mixing zone was a cylindrical cup, with liquid inlets on both sides at the bottom, and was separated from the settling zone by an emulsion overflow and a baffle. The settling zone had four coalescence plates. The volume of the mixing zone was ~120 mL and the volumes of the settling zones were ~100 mL, resulting in a total holdup volume of ~220 mL.

This glass mixer was soaked in 10% nitric acid for at least 12 h before use, and the gas dispersion tube was soaked in aqua regia for the same time, then sonicated in Milli-Q water 3 times sequentially, each for 20 minute durations. The use of a glass unit allowed for better monitoring of the mixing zone as well as a stricter level control in the settling zone. Magnetic stir bars (1") were used to stir phases in the mixing zone of both mixer-settles at a rate of 600 rpm.

*Priming:*

Surge tanks in the flow system were charged with the appropriate solutions, shown in Table S1. The 20 mM of quinone dissolved in the organic phases was prepared by shaking 5 vol% of 1 M aqueous AQDSNa<sub>2</sub> in 0.1 M HClO<sub>4</sub> with the organic phase.

**Table S1.** Priming solutions in surge tanks.

Tank	Solution	Volume (mL)
S-1	0.1 M NaOH (aq)	150
S-2	20 mM AQ-2,7-DS / 0.1 M HClO <sub>4</sub> (aq)	150
S-3	20 mM AQ-2,7-DS / 0.1 M TBACl (hexanol)	150
S-4	20 mM AQ-2,7-DS / 0.1 M TBACl (hexanol)	150
PL	Water w/stabilizer (1 mM Na <sub>2</sub> EDTA, 3 mM citric acid)	2000*

\*When running the closed peroxide loop, 150 mL of water with stabilizer is used.

The first mixer-settler, **MS-1**, was primed by syringe addition of 100 mL of 20 mM AQDS / 0.1 M HClO<sub>4</sub> and 100 mL of 20 mM AQDS / 0.1 M TBACl/1-hexanol. The second mixer-settler, **MS-2**, was primed by syringe addition of 100 mL of stabilized water and 100 mL 0.1 M TBACl/hexanol. The pumps were run at 10 mL min<sup>-1</sup> for 20 mins to allow the system to reach equilibrium before electrochemistry or O<sub>2</sub> sparging were commenced. Tanks S-2, S-3 and S-4 were constantly bubbled with N<sub>2</sub> to prevent oxygen from **MS-2**, carried by the organic phase, from entering the electrochemical cell during the operation of the system. The flow system was kept at the ambient temperature of 20–22°C without any heating or cooling.

### *H<sub>2</sub>O<sub>2</sub> generation:*

A set constant potential was applied across the cell concurrent with the commencement of O<sub>2</sub> bubbling. In the anodic half-cell, water is electrolyzed to oxygen and protons. Oxygen is vented out of the anolyte in S-1. The ionic current flows across the bipolar membrane between the anodic and cathodic half-cells. In the cathodic half-cell the quinone, AQDSNa<sub>2</sub>, undergoes two-electrons, two-proton reduction to the corresponding hydroquinone, AQDSH<sub>2</sub>Na<sub>2</sub>. The catholyte stream carries AQDSH<sub>2</sub>Na<sub>2</sub> to MS-1 where it is contacted with 0.1 M TBACl/1-hexanol. Both reduced and oxidized quinones partition among the two phases according to the equilibrium concentrations shown in Fig 3b. The organic phase, now enriched with hydroquinone, is pumped into MS-2 where it is contacted with water and sparged with oxygen. A three-phase reaction takes place, where O<sub>2</sub> dissolves in the aqueous phase and diffuses to the aqueous-organic interface where it is reduced to H<sub>2</sub>O<sub>2</sub> by the hydroquinone in the organic phase, regenerating the original quinone. The flow rate of oxygen was maintained at 10 mL min<sup>-1</sup> to achieve the complete oxidation of the quinone; excess gas leaves the mixing zone of MS-2 through the headspace outlet port. Although this optimization is beyond the scope of the current study, we stress that the flow rates of the liquid phases, the sizing of the mixing zone, and the mixing rate can all be optimized to achieve full oxidation of quinone at a minimum O<sub>2</sub> flow rate.



### Quantitative analysis:

The flow rates of the streams were changed for the different experiments as seen in Table S2.

**Table S2.** Flow rates for each experiment.

Experiment	Flow rates (mL min <sup>-1</sup> )				$\tau$ (min)	
	Anolyte	Catholyte	Organic	Water	Water	Quinone
Variation of current (Figure 6b)	10	10	10	10	11	70
Steady-state H <sub>2</sub> O <sub>2</sub> production (Figure 6a)	10	10	10	10	11	70
Looping (Figure S11)	10	10	10	10	11	70
Flow rate variation (Figure 6c)	10	10	10	20	5.5	70
	10	10	10	10	11	70
	10	10	10	5	22	70
	10	10	10	2.5	44	70
	20	20	20	2.5	44	35
	40	40	20	2.5	11	17.5

Residence time,  $\tau$ , of a stream in a unit is obtained as the ratio of holdup volume,  $V$ , of the unit to the flow rate,  $F$ , of the stream.

$$\tau = \frac{V}{F} \quad (1)$$

The residence time of the water stream was calculated by using the water flow rate and half the total holdup volume in MS-2 (110 mL) since equal volumes of the organic and aqueous phases were maintained in the mixer-settlers. As for the residence time of the quinone, which here refers to the time it takes for a molecule of quinone to complete the entire process once, the half holdup volumes of both mixer-settlers were used as well as tanks S-2, S-3, S-4, the electrochemical cell, and the connecting tubing, resulting in a total holdup volume of ~700 mL. For flow rates, since all quinone carrying streams were flowing at the same rate in all the experiments, the catholyte flow rate was used.

### Calculation of system performance metrics

H<sub>2</sub>O<sub>2</sub> was quantified by iodometric titration, generating I<sub>2</sub> from the addition of an aliquot of solution to KI and H<sub>2</sub>SO<sub>4</sub> and quenching the formed I<sub>2</sub> with 0.1 M Na<sub>2</sub>S<sub>2</sub>O<sub>3</sub>, according to a standard procedure.<sup>2</sup> Peroxide titrations were also periodically cross-checked using peroxidase-based semi-quantitative test strips (Millipore MQuant™, 0–100 ppm / 100–1000 ppm, LaMotte InstaTest™ 0–90 ppm, 1 mM = 34 ppm).

The rate of H<sub>2</sub>O<sub>2</sub> production (in μmol min<sup>-1</sup>) was calculated from the measured peroxide concentration, C<sub>H<sub>2</sub>O<sub>2</sub></sub>, (in μM) and the flow rate of the product stream, F<sub>water</sub> (in mL min<sup>-1</sup>).

$$R_{\text{H}_2\text{O}_2} = F_{\text{water}} C_{\text{H}_2\text{O}_2} \quad (2)$$

This value was then normalized to the geometric surface area (25.8 cm<sup>2</sup>) to give a rate density, v<sub>d</sub>, in μmol min<sup>-1</sup> cm<sup>-2</sup> as reported in Fig. 6a and 6b.

The current density, *j*, (in mA cm<sup>-2</sup>) was calculated from the ratio of the current, *I*, (in mA) and the geometric area of the electrode 2'' × 2'' = 25.81 cm<sup>2</sup>:

$$j = \frac{I}{25.81} \quad (3)$$

The Faradaic efficiency (% H<sub>2</sub>O<sub>2</sub> production) was calculated from the ratio of the calculated rate of peroxide production, R<sub>H<sub>2</sub>O<sub>2</sub></sub>, to the rate calculated under the assumption that all electrons contribute to peroxide synthesis, R<sub>H<sub>2</sub>O<sub>2</sub>,th</sub>:

$$FE = \frac{R_{\text{H}_2\text{O}_2}}{R_{\text{H}_2\text{O}_2,\text{th}}} \quad (3)$$

Where,

$$R_{\text{H}_2\text{O}_2,\text{th}} = (n_e F)^{-1} (10^6 \text{ } \mu\text{mol/mol}) (10^{-3} \text{ A/mA}) (60 \text{ s/min}) I = 0.311 I \quad (4)$$

In this equation, *I* is the measured current in mA, *F* is Faraday's constant, 96485 s A mol<sup>-1</sup> and *n<sub>e</sub>* is 2 for the two-electron stoichiometry of O<sub>2</sub> reduction to H<sub>2</sub>O<sub>2</sub>.

In order to derive iR-free values for cell potential, we estimated the slope of the I-V diagram shown in Figure S10. This plot is nonlinear indicating a mixture of resistive and non-resistive components. The tangent of the high current region corresponding to 5 Ω effective resistance. As a conservative lower bound, we take 90% of this value (4.5 Ω), to compensate for iR losses in the cell according to the following equation:

$$V_{\text{corr}} = V - 4.5 I \quad (5)$$

The power density (in  $\text{mW cm}^{-2}$ ) was calculated from the current density,  $j$ , and the iR-free cell potential,  $V$ .

$$P = jV \quad (6)$$

The energy efficiency was calculated from the thermodynamic cell potential for  $\text{H}_2\text{O}_2$  formation from water and  $\text{O}_2$  (Equation 2 in main text), 0.529 V, and the fractional Faradaic efficiency

$$E = \left( \frac{0.529\text{V}}{V} \right) (\text{FE}) \quad (7)$$

### CO<sub>2</sub> Footprint Calculation

Steam methane reforming, SMR, followed  $\text{H}_2\text{O}_2$  generation via the AQ process, has a molar stoichiometry of 1:4,  $\text{CO}_2:\text{H}_2$ , or a mass ratio of 0.65:1,  $\text{CO}_2:\text{H}_2\text{O}_2$ . Thus, 4.3 Mt of  $\text{H}_2\text{O}_2 = 2.8$  Mt  $\text{CO}_2$  from SMR alone.

### Reverse Osmosis Energy Calculations

To estimate the energy cost of reverse osmosis (RO) separation of  $\text{H}_2\text{O}_2$  from the electrolyte, we considered a electrochemical peroxide generation system that produces a  $\sim 500$  ppm (15 mM) of  $\text{H}_2\text{O}_2$  in 0.1 M ionic strength aqueous electrolyte.<sup>2</sup> An RO process could be used to reduce the ionic strength to, for example, 0.01 M and would lead to a following energy cost.<sup>3</sup>

For a process at  $T = 298$  K, the osmotic pressure is given by:

$$\pi = 1.12T \sum m_i \text{ in psia where } m_i \text{ is the molarity of the ions.}^4$$

Hence  $\pi_{\text{Feed}} = 66.7$  psia,  $\pi_{\text{Permeate}} = 0.667$  psia, and  $\Delta\pi = 66$  psia or  $\sim 4.5$  atm

In RO processes, typically,  $\Delta P \cong (2-4)\Delta\pi$

And the pump work rate is given by  $\dot{w} = Q\Delta P$  where  $Q$  is the flow rate.

To achieve the separation of 1 kg of  $\text{H}_2\text{O}_2$  from the 0.1 M ionic strength electrolyte,  $2 \text{ m}^3$  of solution needs to be treated. By cancelling the time component from the equation, the total work done is  $w = 0.5 - 1$  kWh/kg.

This is an approximation, which does not account for the energy cost of the rejected brine, which has  $\text{H}_2\text{O}_2$  at near feed concentrations. It also does not take into account other pressure drops due to specialty membranes and other protective films, which prevent, or slow down, membrane degradation via oxidation or parasitic reactions with the caustic electrolyte media.

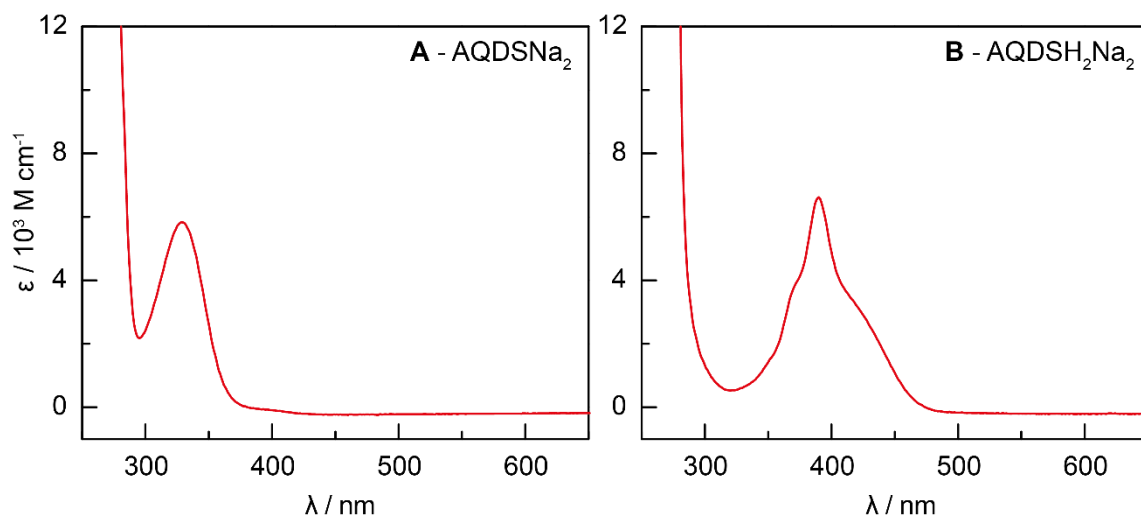


**Figure S1.** Representative aqueous UV-Vis spectra of AQDSNa<sub>2</sub> (A) and AQDSH<sub>2</sub>Na<sub>2</sub> (B)

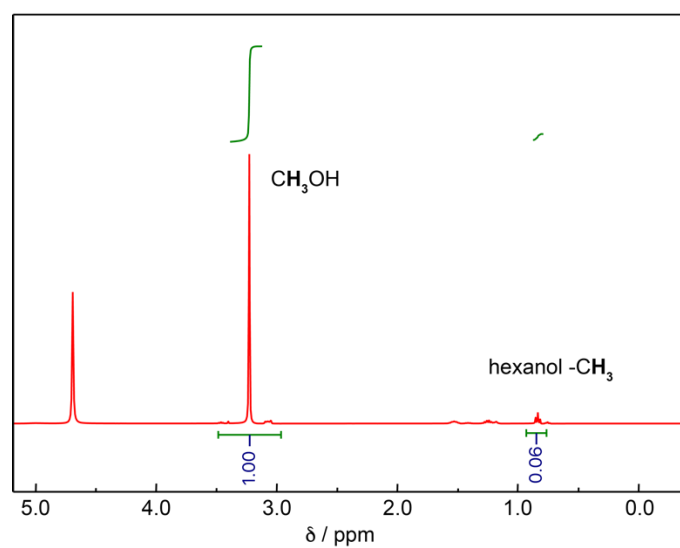


**Figure S2.** <sup>1</sup>H NMR spectrum of D<sub>2</sub>O after mixing with 0.1 M TBACl/1-hexanol, with 0.5% methanol (0.12 M) subsequently added to quantify 1-hexanol transfer.

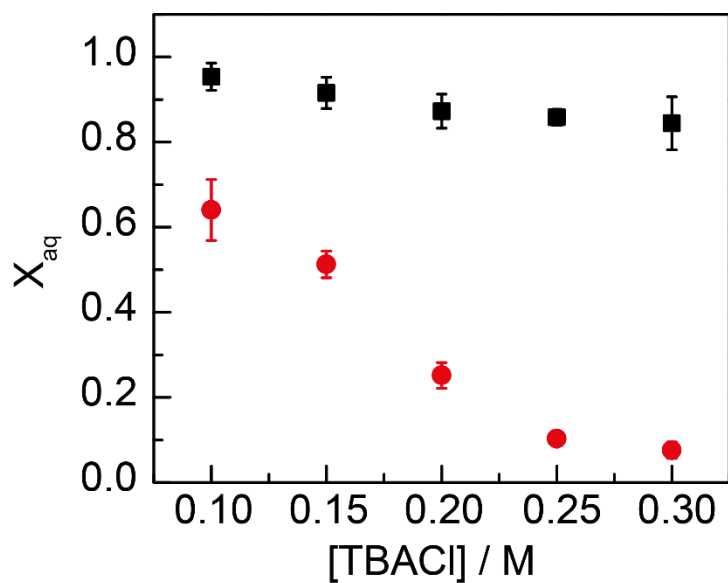


**Figure S3.** Phase transfer partition coefficient,  $X_{aq}$ , for 0.1 M HClO<sub>4</sub>/20 mM AQDSNa<sub>2</sub> (red circles) and 0.1 M HClO<sub>4</sub>/20 mM AQDSNa<sub>2</sub>H<sub>2</sub> (black squares) in contact with TBACl in CH<sub>2</sub>Cl<sub>2</sub>.

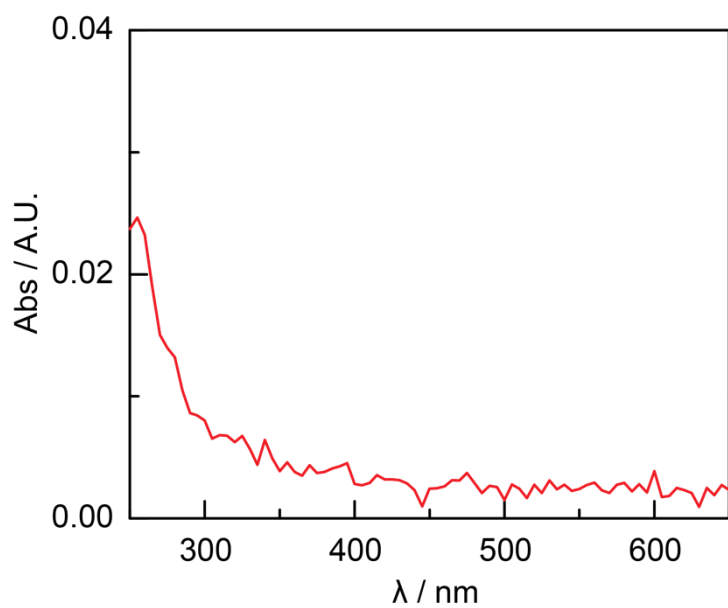


**Figure S4.** UV-Vis spectrum of electrolyte-free water upon mixing with AQDSH<sub>2</sub>TBA<sub>2</sub>/1-hexanol in 0.1 M TBACl and oxygen, showing <1% transfer of AQDSH<sub>2</sub>TBA<sub>2</sub> or AQDSTBA<sub>2</sub>.

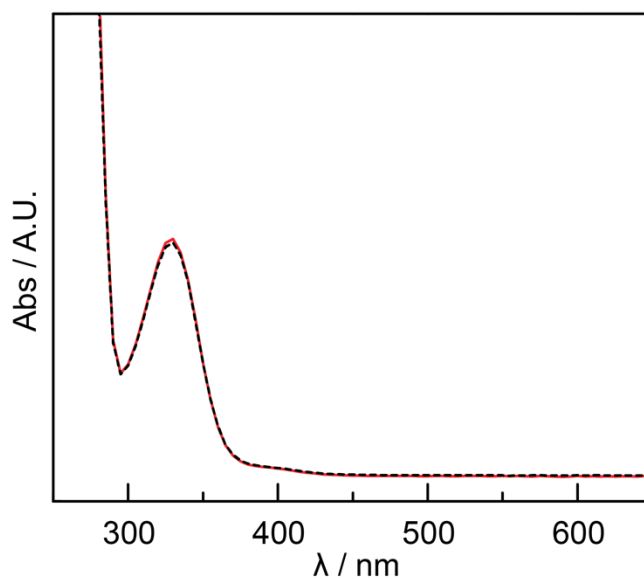


**Figure S5.** UV-Vis spectrum of AQDSNa<sub>2</sub> before (red line) and after (black dashed line) a cycle of reduction, phase transfer, reoxidation, and back transfer.

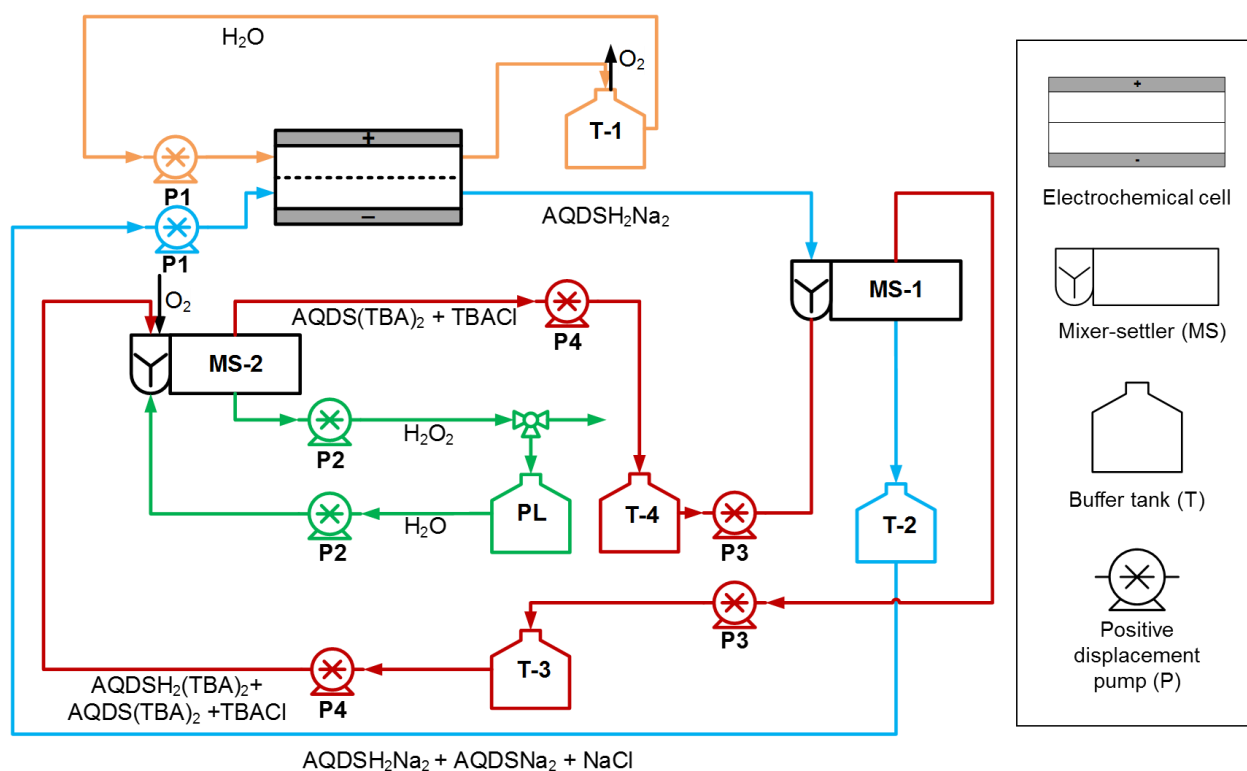


**Figure S6.** Process flow diagram illustrating the flow of the different phases through the electrochemical cell, mixer-settlers and surge (buffer) tanks. The color of the stream indicates an independent phase: **blue** represents the aqueous catholyte circuit, **orange** is the anolyte circuit, and **red** is the organic phase circuit. **Green** represents the peroxide circuit, which can flow in an open circuit or as a closed loop in the peroxide loop tank (PL).

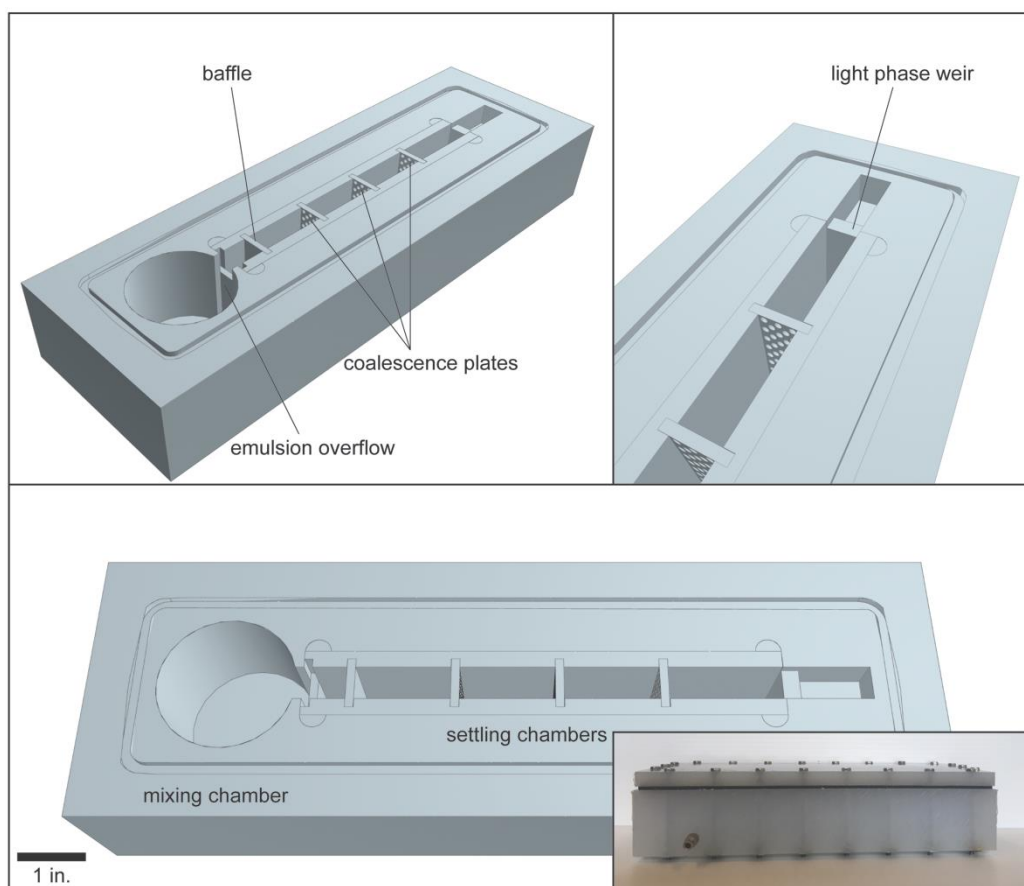


**Figure S7.** Diagram of the first mixer-settler, **MS-1**. Inset: picture of the polypropylene machined unit.

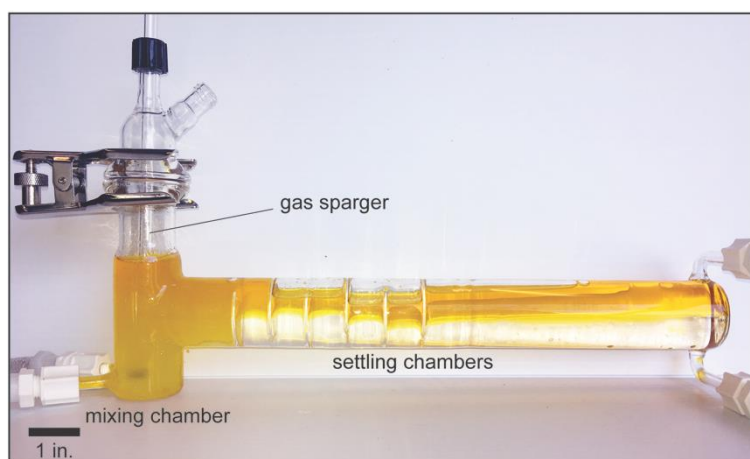


**Figure S8.** Picture of the second mixer-settler, **MS-2**, with the 1-hexanol-water emulsion being sparged with  $O_2$  in the mixing chamber and the phase separation occurring in the settling chambers.

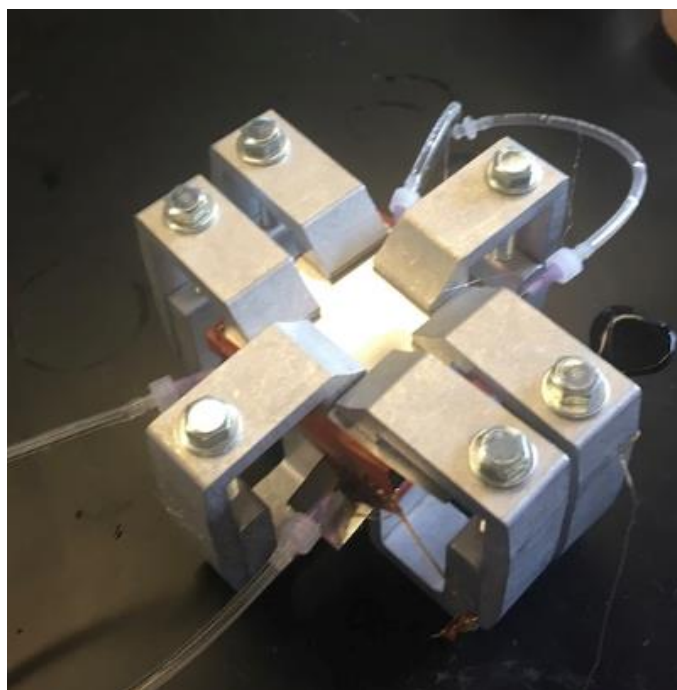
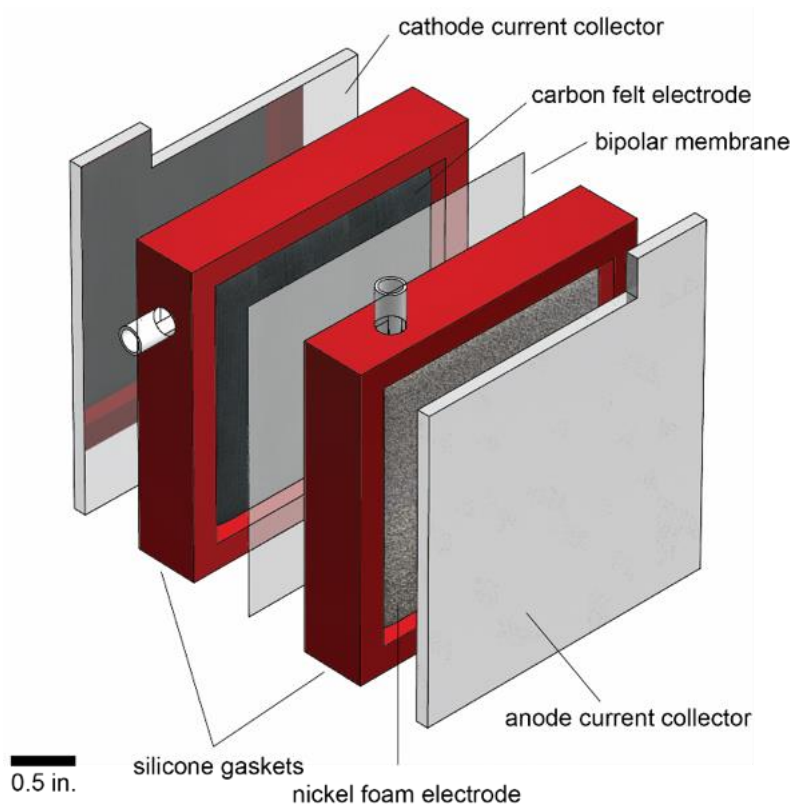


**Figure S9.** Schematic of the electrochemical cell (top). Ports, like those seen on the silicone gaskets, allow flow of catholyte and anolyte in and out of the cathodic and anodic half-cells, respectively (bottom).



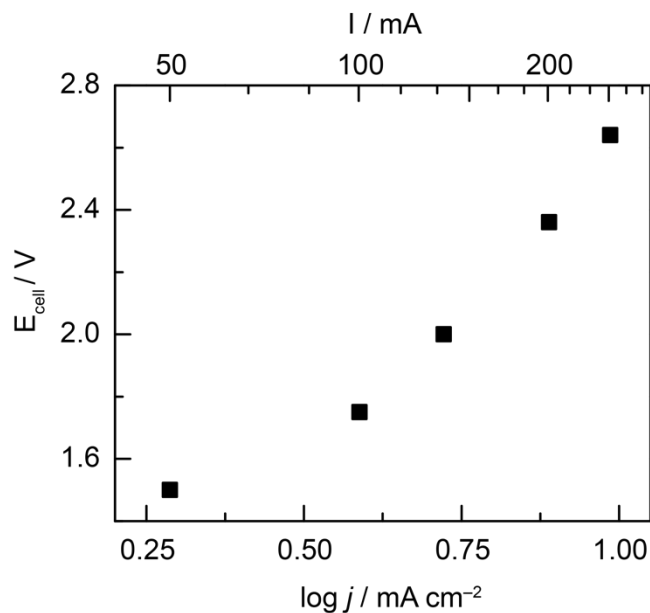


**Figure S10.** Current-potential relationship of cell operated in the flow configuration.

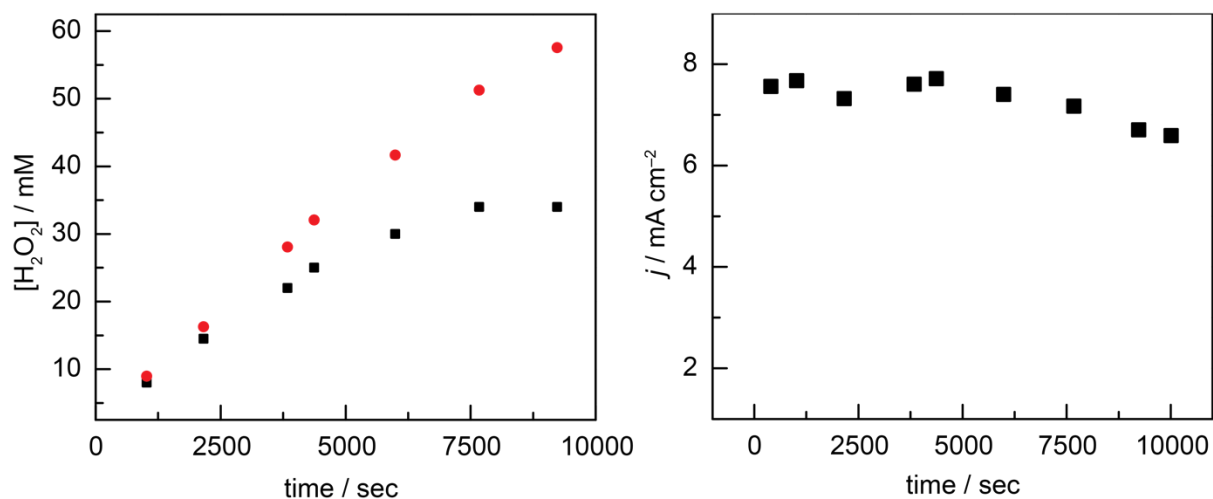


**Figure S11. Left:** Increase of H<sub>2</sub>O<sub>2</sub> concentration (black squares) with time in 150 mL water looped in stream (3) (see Figure 5). The cell voltage was set at 2.25 V, flow rates of (2) and (3) (see Figure 5) were 10 mL/min and 2.5 mL/min respectively, red circles show theoretical H<sub>2</sub>O<sub>2</sub> production from current density assuming no decomposition upon looping. **Right:** Current density vs time (from same experiment) showing relatively constant quinone re-reduction.

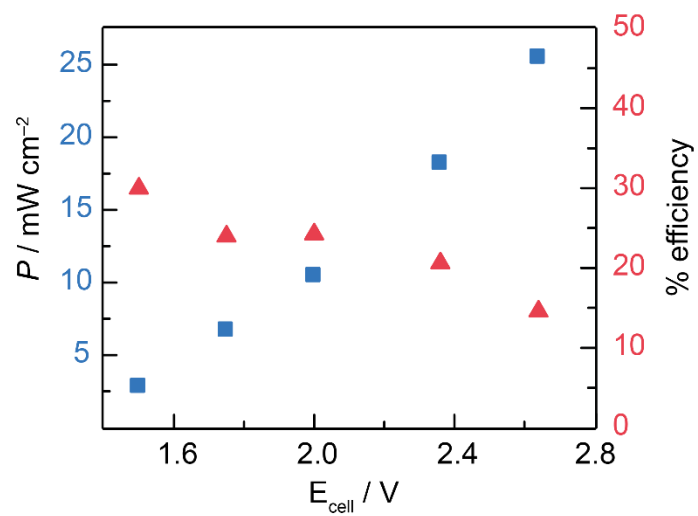


**Figure S12.** Power densities (left axis) of the electrochemical cell and energy efficiencies (right axis) for the production of hydrogen peroxide versus cell voltage. These data incorporate the uncompensated cell resistance.

## References

1. Gamage, R.S.K.A., McQuillan, A.J., and Peake, B.M. (1991). Ultraviolet–visible and electron paramagnetic resonance spectroelectrochemical studies of the reduction products of some anthraquinone sulphonates in aqueous solutions. *J. Chem. Soc. Faraday Trans.* *87*, 3653–3660.
2. Chen, Z., Chen, S., Siahrostami, S., Chakthranont, P., Hahn, C., Nordlund, D., Dimosthenis, S., Nørskov, J.K., Bao, Z., and Jaramillo, T.F. (2017). Development of a reactor with carbon catalysts for modular-scale, low-cost electrochemical generation of H<sub>2</sub>O<sub>2</sub>. *React. Chem. Eng.* *2*, 239–245.
3. Kezia, K., Lee, J., Ogieglo, W., Hill, A., Benes, N.E., and Kentish, S.E. (2014). The transport of hydronium and hydroxide ions through reverse osmosis membranes. *J. Membr. Sci.* *459*, 197–206.
4. Applegate, L.E. (1984). Membrane separation processes. *Chem. Eng.* *12*, 64–89.